The angular distribution of energetic electron and X-ray emissions from triggered lightning leaders

M. M. Schaal,[1] J. R. Dwyer,[1] H. K. Rassoul,[1] J. D. Hill,[2] D. M. Jordan,[3] and M. A. Uman[3]

Received 5 February 2013; revised 26 September 2013; accepted 7 October 2013; published 23 October 2013.

[1] We investigate individual X-ray bursts from lightning leaders to determine if energetic electrons at the source (and hence X-rays) are emitted isotropically or with some degree of anisotropy. This study was motivated by the work of Saleh et al. (2009), which found the falloff of X-rays in concentric radial annuli, covering all azimuthal directions in each annulus, from the lightning channel to be most consistent with an isotropic electron source. Here we perform a statistical analysis of angular and spatial distributions of X-rays measured by up to 21 NaI/PMT detectors at the International Center for Lightning Research and Testing site for 21 leader X-ray bursts from five leaders (including four dart-stepped leaders and one dart leader). Two procedures were used to complete this analysis. Procedure 1 found the first-order anisotropy, and procedure 2 tested whether or not the angular distribution was consistent with an isotropic distribution. Because higher-order anisotropies could be present in the data, a distribution that is not isotropic does not necessarily have a significant first-order anisotropy. Using these procedures, we find that at least 11 out of 21 X-ray bursts have a statistically significant first-order anisotropy, and hence those 11 are inconsistent with an isotropic emission. The remaining 10 bursts do not have significant first-order anisotropy. However, of those 10 bursts, 9 are inconsistent with isotropic emission, since they exhibit significant higher-order anisotropies. Since Saleh et al. (2009) did not consider anisotropies in the azimuthal direction, these new measurements of anisotropy do not necessarily contradict that work. Indeed, our analysis supports the finding that the X-ray emissions from lightning are inconsistent with a vertically downward beam. The level of anisotropy of the runaway electrons is important because it provides, in principle, information on the streamer zone in front of the leader and the electric field near the lightning leader tip.

Citation: Schaal, M. M., J. R. Dwyer, H. K. Rassoul, J. D. Hill, D. M. Jordan, and M. A. Uman (2013), The angular distribution of energetic electron and X-ray emissions from triggered lightning leaders, *J. Geophys. Res. Atmos.*, *118*, 11,712–11,726, doi:10.1002/2013JD019619.

1. Introduction

[2] Much is not known about the properties of lightning leaders, including the angular distribution of energetic electrons and X-rays emitted by them. Prior to 2001, confirmation of X-ray emission from lightning processes were questionable due to incomplete measurements and the random nature of natural lightning [*Suszcynsky et al.*, 1996]. The literature on the properties of the leader source and the characteristics of X-ray and electron emission from the source region will be reviewed in this section.

[1]Department of Physics and Space Sciences, Florida Institute of Technology, Melbourne, Florida, USA.
[2]Team QNA, ESC-25, Kennedy Space Center, Florida, USA.
[3]Department of Electrical and Computer Engineering, University of Florida, Gainesville, Florida, USA.

Corresponding author: M. M. Schaal, Department of Physics and Space Sciences, Florida Institute of Technology, Melbourne, FL 32901, USA. (meagan.schaal@gmail.com)

2169-897X/13/10.1002/2013JD019619

[3] The first coincidence of stepped leader light pulses with electric field pulses was demonstrated by *Beasley et al.* [1983]. Electric field pulses have been commonly observed during natural lightning stepped leader steps [*Kitagawa*, 1957a; *Krider and Radda*, 1975; *Krider et al.*, 1977; *Cooray and Lundquist*, 1985; *Rakov and Uman*, 2003; *Howard et al.*, 2008, 2010; *Hill et al.*, 2012] and are thought to occur from the step formation process. Furthermore, *Krider et al.* [1977] ascertained, through modeling, that the peak step current was at least 2–8 kA close to the ground and the minimum charge in the step formation was about $1–4\times10^{-3}$ C. *Howard et al.* [2010] inferred similar peak currents and derived current waveforms for two steps.

[4] *Gorin et al.* [1976], using laboratory spark experiments, determined that the formation of a step occurred predominantly at the tip in the leader channel. In front of the leader tip of a negatively charged leader channel, a streamer zone, composed of positive and negative streamers, was found to exist. These streamers appeared to originate from an isolated space stem, or space leader, a plasma formation ahead of the leader tip. The leader step was suggested

Table 1. The χ^2_ν, Probability, Pearson's Probability, the Magnitude of Anisotropy (A), and Direction of Anisotropy (ϕ_0, in Degrees) Results for Each X-Ray Burst From the Dart-Stepped Leader From UF 07-07

X-Ray Burst	χ^2_ν	P	P_p	A	ϕ_0
B	28.44	0	0.00005	3.178 ± 0.632	102.67 ± 15.16
C	2.004	0.075	0.0507	1.243 ± 0.593	9.99 ± 29.45
D	1.972	0.079	0.0138	0.794 ± 0.566	23.24 ± 35.51
E	10.66	0	0.00005	0.665 ± 0.403	329.11 ± 23.75
F	19.84	0	0.0098	0.847 ± 0.311	349.38 ± 9.47
G	6.264	0	0.0036	0.687 ± 0.466	277.38 ± 34.46
H	7.937	0	0.00005	0.755 ± 0.726	281.75 ± 43.791
I	23.76	0	0.00005	1.240 ± 0.520	100.99 ± 23.75
J	2.945	0.010	0.074	0.654 ± 0.824	253.73 ± 53.36
L	5.598	0	0.00005	0.203 ± 0.885	119.25 ± 103.11
O	14.34	0	0.00005	0.841 ± 0.523	63.96 ± 32.66
Q	320.36	0	0.00005	2.098 ± 0.507	104.84 ± 12.64
S	3.96	0.0014	0.00005	0.762 ± 0.756	31.32 ± 45.72

to form when the end of an upward moving positive space leader tip makes contact with the tip of a downward moving negative leader channel. As a result, a burst of streamers, i.e., a coronal flash, is produced in front of the leader tip below the space leader. The local electric field near the tip is thought to provide the initial steering direction that the streamers take, and a new space stem then forms out of those streamers, thus allowing the process to be repeated.

[5] Runaway electron production, which is thought to form in the streamer zone, during the time of the coronal flash, generates X-rays through bremsstrahlung emission [*Gurevich*, 1961; *Gurevich et al.*, 1992; *Gurevich and Zybin*, 2001; *Dwyer et al.*, 2003; *Dwyer*, 2004; *Moss et al.*, 2006; *Kochkin et al.*, 2012]. Further details involving the characteristics of the emission of electrons and X-rays from the source region and also the orientation of the electric field near the leader tip are poorly understood.

[6] The first definitive detection of energetic radiation associated with lightning was measured by *Moore et al.* [2001], at Langmuir Laboratory in New Mexico, who detected energetic emissions from three natural cloud-to-ground (CG) lightning leaders in coincidence with changes in electric field. These emissions began 1 to 2 ms prior to the start of the return stroke and continued to the onset of the return stroke.

[7] *Dwyer et al.* [2003], at the International Center for Lightning Research and Testing (ICLRT) in Florida, measured energetic radiation during the dart and dart-stepped leader phase of rocket-and-wire triggered lightning. They found that the dart-stepped leaders emitted energetic radiation as much as 160 μs before the start of the return strokes. *Dwyer et al.* [2004a] showed, through the use of attenuators, that nearly all of the energetic emission was made of X-rays and that the emission reached to about 250 keV. Additionally, the bottom 50 m of the leader channel was determined to be the origin of most of the observed X-ray emission, and the X-ray emission increased as the lightning leader tip neared the ground. X-rays from rocket-and-wire triggered dart-stepped leaders were observed to arrive in individual bursts, with each X-ray pulse enduring less than 1 μs. *Dwyer et al.* [2005] measured X-ray emissions associated with natural CG stepped leaders. The X-ray emission was strikingly similar to the X-ray bursts from dart-stepped leaders, indicating a shared production mechanism. *Dwyer et al.* [2005] also reported that X-rays are most often emitted during the formation of lightning leader steps and are closely linked to the stepping process.

[8] *Saleh et al.* [2009] further characterized the properties of X-ray emission from rocket-triggered lightning at the ICLRT. Particularly, one rocket-triggered dart-stepped leader (UF 07-07 Leader (L)1) and two rocket-triggered dart leaders were examined to acquire a modeled X-ray energy spectrum, an electron luminosity function, and an empirical relation for the radial (around the lightning source leader) X-ray distribution. UF stands for University of Florida and refers the year of the triggered flash, e.g., 07, and the triggered flash number, e.g., 07 for that year. *Saleh et al.* [2009] measured the deposited energy at the ground and determined that it falls off proportional to $\exp[-r/120]/r$ where r is the cylindrical radial distance in meters from the lightning leader channel. They also found that the electron source of the X-ray emission was not beamed downward but, on average, emitted isotropically in the bottom hemisphere with an average electron energy of about 1 MeV. Using Monte Carlo simulations, the average energetic electron luminosity was found to be on the order of 10^{16} electrons/s for UF 07-07 Leader 1. The maximum X-ray luminosity was deduced to be on the order of 10^{15} s^{-1}. Furthermore, *Dwyer et al.* [2010] estimated that there are about 10^{11} energetic electrons emitted per step.

[9] Although some questions regarding X-ray emission from lightning leader processes have been answered

Table 2. The χ^2_ν, Probability, Pearson's Probability, the Magnitude of Anisotropy (A), and Direction of Anisotropy (ϕ_0, in Degrees) Results for Each X-Ray Burst From the Dart Leader From UF 10-06

X-Ray Burst	χ^2_ν	P	P_p	A	ϕ_0
A	0.357	0.878	0.761	2.202 ± 2.998	44.04 ± 104.89
B	11.2	0	0.00005	1.085 ± 1.392	170.72 ± 67.02

Table 3. The χ^2_ν, Probability, Pearson's Probability, the Magnitude of Anisotropy (A), and Direction of Anisotropy (ϕ_0, in Degrees) Results for Each X-Ray Burst From the Dart-Stepped Leader From UF 10-23

X-Ray Burst	χ^2_ν	P	P_p	A	ϕ_0
A	6.522	0	0.00005	0.014 ± 0.689	22.13 ± 139.70
B	14.77	0	0.00005	0.480 ± 0.756	233.93 ± 57.73
C	5.879	0.0383	0.0013	0.418 ± 0.863	156.57 ± 69.28
D	2.75	0.0739	0.031	0.633 ± 1.092	328.64 ± 69.05

(e.g., approximate characteristic energy and luminosity of electrons and X-rays), the angular distribution of electron and X-ray emission for individual bursts has not been well-established [*Dwyer et al.*, 2012], since *Saleh et al.* [2009] only measured the sum of many individual X-ray bursts. This study was motivated by the work of *Saleh et al.* [2009], which found the falloff of X-rays in concentric radial annuli, covering all azimuthal directions in each annulus, from the entire lightning channel to be most consistent with an isotropic electron source. Since *Saleh et al.* [2009] did not consider the azimuthal direction individually, it would be beneficial to determine if X-ray bursts within the lightning channel are also consistent with an isotropic electron source. The level of anisotropy of the runaway electrons is important because it provides, in principle, information on the streamer zone in front of the leader and the electric field near the lightning leader tip.

[10] In this paper, we report new details about the angular distribution of X-ray bursts from rocket-triggered leaders as measured by the Thunderstorm Energetic Radiation Array (TERA). TERA observes energetic radiation in the form of X-rays and gamma-rays (energies varying from 30 keV to several MeV) from natural and rocket-and-wire triggered lightning. TERA is located at the ICLRT at the Camp Blanding Army National Guard Base in Florida and is jointly operated by the University of Florida and Florida Institute of Technology. The facility spans an area of about 1 km^2 and, since 2002, contains instruments to measure X-rays from lightning. Together with TERA, another instrument array, the Multiple Station Experiment (MSE), records the horizontal magnetic field using loop antennas, the vertical component of electric fields and their derivatives using wideband flat plate antennas, and optical measurements. Additionally, the leader source positions of the radiated electric field derivative (dE/dt) signals and the X-ray signals are determined in 3-D by the 10 station TERA/MSE network through a time-of-arrival (TOA) technique. Further details regarding the TOA network can be found in *Hill et al.* [2012] and *Hill* [2012].

[11] Here we present evidence of significant first-order anisotropy (or a burst of X-rays in one azimuthal direction) in the X-ray emission of 11 out of 21 leader X-ray bursts. The remaining 10 bursts do not have significant first-order anisotropy. However, of those 10 bursts, 1 is consistent with having an isotropic distribution while the remaining 9 have significant higher-order anisotropies and are inconsistent with isotropic emission.

2. Instrumentation

[12] TERA contains 25 separate aluminum boxes specifically designed to exclude light, water, and radio frequency (RF) noise [*Dwyer et al.*, 2003, 2004a, 2005]. Each box contains either one or two NaI(Tl)/PMT (photomultiplier tube) detectors with the essential electronics and fiber optics for control [*Dwyer*, 2008].

[13] Each TERA box is remotely operated through a group of PIC controllers that are linked to the launch control trailer through 62.5 μm fiber optics. Within each aluminum box, Opticomm FM fiber optic transmitters send PMT anode signals to the acquisition system that is located in a shielded launch control. Corrections have been made for fiber optic propagation delays in the analysis.

[14] The digital storage oscilloscopes recording the TERA anode signals are triggered by incident current measuring at least 6 kA at the rocket launcher for rocket-triggered lightning or by two optical instruments at opposite locations of the ICLRT for natural lightning [*Howard et al.*, 2010]. The incident current is measured under the rocket launcher with a noninductive T&M Research R-7000-10 current viewing resistor (CVR) with a bandwidth from DC to 8 MHz [*Hill et al.*, 2012]. For 2010, two 16-channel Yokogawa DL 716 Scopecorders and one 16-channel Yokogawa DL 750 Scopecorders together recorded the anode signals from the 36 PMT channels through fiber optic cables. For 2007, two 16-channel Yokogawa DL 750 Scopecorders were used. Two seconds of X-ray data with 1 s of pretrigger sampling are measured at a sampling rate of 10 million samples per second for the DL 750 scopes, while the DL 716 scopes record 0.8 s of pretrigger sampling and 1.6 s of data. All three scopes are digitized with 12 bit amplitude resolution. All of the other instruments, including the TOA network, are recorded using a similar method, albeit with higher digitization rates. Additional details about TERA are described in *Saleh et al.* [2009] and *Schaal et al.* [2012].

3. Modeling

[15] Bremsstrahlung X-rays and runaway electrons are produced, from triggered and natural lightning, in strong

Table 4. The χ^2_ν, Probability, Pearson's Probability, the Magnitude of Anisotropy (A), and Direction of Anisotropy (ϕ_0, in Degrees) Results for the Leader X-Ray Bursts Analyzed From UF 10-20 and UF 10-24

X-Ray Burst	χ^2_ν	P	P_p	A	ϕ_0
UF 10-20 L4	1.92	0.0874	0.00005	0.722 ± 0.834	43.60 ± 23.20
UF 10-24 L6	3.34	0.0051	0.00005	0.687 ± 0.928	357.73 ± 25.91

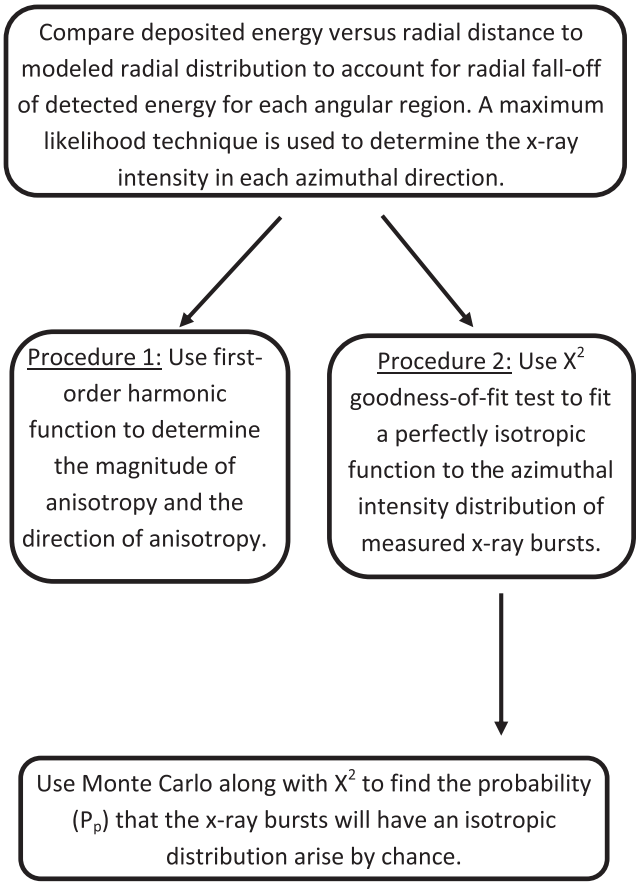

Figure 1. A flowchart of the analysis performed in this report.

electric fields as the energetic electrons interact with air molecules [*Dwyer et al.*, 2005]. To simulate these mechanisms, detailed Monte Carlo models of runaway electron propagation of air were used. When using TERA, the effect of X-rays interacting with air molecules are important because the array spans such a large area.

[16] The Monte Carlo simulation includes all interactions affecting energetic electrons (and positrons), which include Møller scattering for secondary electron production, energy losses through ionization and atomic excitation, and electron scattering [*Dwyer et al.*, 2003; *Dwyer*, 2004, 2007; *Dwyer and Smith*, 2005]. Photon (X-ray and gamma-ray) interactions including pair production, photoelectric absorption, and Rayleigh and Compton scattering are also modeled. Additionally, bremsstrahlung production of X-rays and gamma-rays from all positrons and secondary electrons and gamma-rays from positron annihilation are also modeled. Since we are simulating the interactions with particle detectors positioned at ground level, absorption and backscatter of X-rays with the soil are included. Effects from the instrument itself, including aluminum and lead, are also implemented within the Monte Carlo model.

[17] Because X-rays are associated with negative lightning leader stepping in natural and triggered lightning, the electron source is expected to be positioned in or near a strong electric field at the leader tip. The energetic electron spectrum is inferred to be initially of the form $dN_e/dK \propto \exp(-K/K_0)$ where K is the kinetic energy of the runaway electrons and K_0 is set to 1 MeV [*Lehtinen et al.*, 1999; *Dwyer*, 2004]. Using this energy spectrum, the runaway electrons are propagated through air where both the ambient electric and magnetic fields are set to zero. The Earth's magnetic field has been determined to have no significant impact on the model's results for X-ray emissions near the ground [*Dwyer and Smith*, 2005].

[18] The models are based on the assumption that a stepped leader radiates electromagnetic pulses, both colocated in three-dimensional coordinate space above the ground. However, only the electron and X-ray emission are modeled in these simulations. This simulation, following *Saleh et al.* [2009], describes the source of X-rays as a point source that propagates in the vertically downward, negative z direction with the same speed as the dE/dt sources. The energetic electrons are injected into the model at the source altitude (determined by the approximate location estimates of the leader tip position based on the approximate downward average leader speed by using TOA source locations, if available, or approximate dart and dart-stepped leader speeds) of the lightning leader and propagated until they lose energy and stop. When integrated over all time, the X-ray

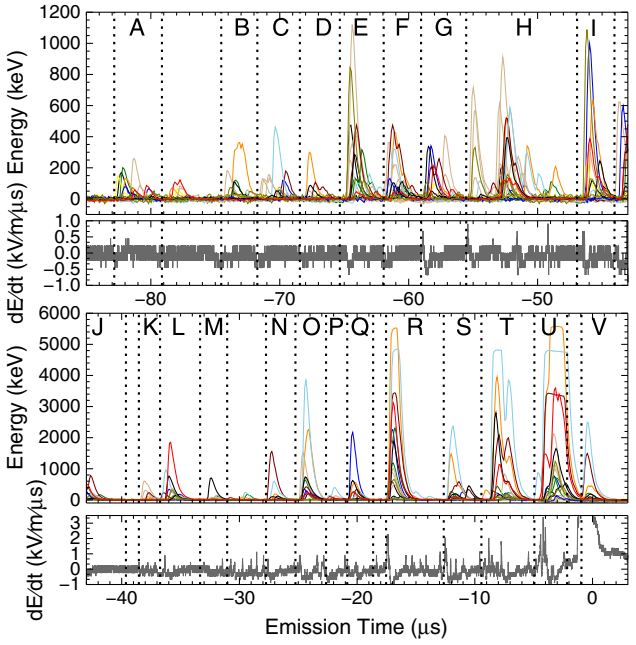

Figure 2. The waveform of X-rays from the dart-stepped leader UF 07-07 converted into energy using a calibration from Cs-137 radioactive source. The electric field derivative waveform is shown below the X-ray waveform. Each color of X-ray pulse displays a separate NaI/PMT detector. The timing has been adjusted to show emission times, so that the distinction between X-ray bursts can be seen. The dashed lines segmenting the X-ray bursts indicate the approximate individual time lengths of each X-ray burst, which were chosen to be about at the start and stop of the X-ray emission for each X-ray burst. The letters at the top of each X-ray burst segment indicate the time frame of each X-ray burst. Times B, C, D, E, F, G, H, I, J, L, O, Q, and S were chosen to be analyzed statistically.

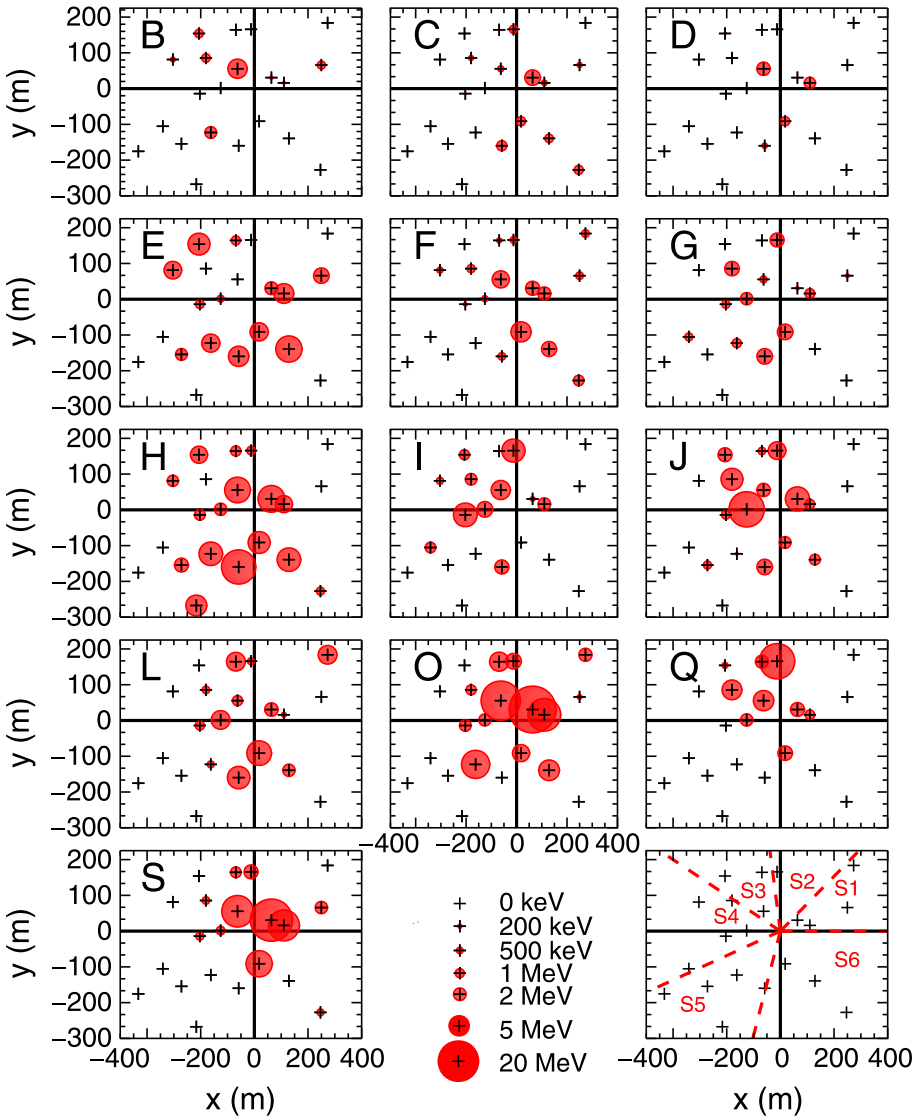

Figure 3. The spatial distribution of energies across the unshielded NaI/PMT detectors from the X-ray bursts of UF 07-07. The plus markers indicate the location of the TERA detectors across the ICLRT site. A north and east headings are labeled as y and x, respectively. The horizontal and vertical black lines at the origin show the position of the launcher. The red circles indicate the total energy deposited in each unshielded NaI/PMT with the area proportional to its energy. The dashed lines (bottom right) indicate which TERA PMTs are located in each azimuthal region (S1, S2, S3, S4, S5, and S6).

sources, therefore, form a vertical line. The origin for this simulation is the strike point of the lightning at the rocket launcher.

[19] An isotropic electron source, based on the results proposed by *Saleh et al.* [2009], was modeled for all five lightning leaders to check consistency with the measured deposited energies. In the simulation, energetic electrons are injected and then lose their energy, mainly through ionization of the air. As they move, they also undergo elastic scattering with air atoms and emit bremsstrahlung X-ray photons. These photons have an energy spectrum of approximately $1/E_{ph}$ times the energy spectrum of the energetic electrons that emit them. They are also emitted with an angular distribution with an angular width (in radians) of approximately $1/\gamma$, where γ is the Lorentz factor of the electron.

[20] The photons are then propagated in the simulation until they are absorbed or fall below an energy of 30 keV, which is about the lower sensitivity limit that the NaI/PMTs can detect when positioned inside the TERA boxes. A ground plane is placed at z = 0 m to collect the X-ray emission from the model, and the simulated data are divided into regions ($\pm$10 m in both the x and y directions from the location of the TERA box) that correspond to the location of each TERA box. Regions of $\pm$10 m were used, instead of the actual TERA box dimensions, to improve statistics.

4. Analysis

[21] *Saleh et al.* [2009] presented evidence of an isotropic electron source averaged over the entire leader channel,

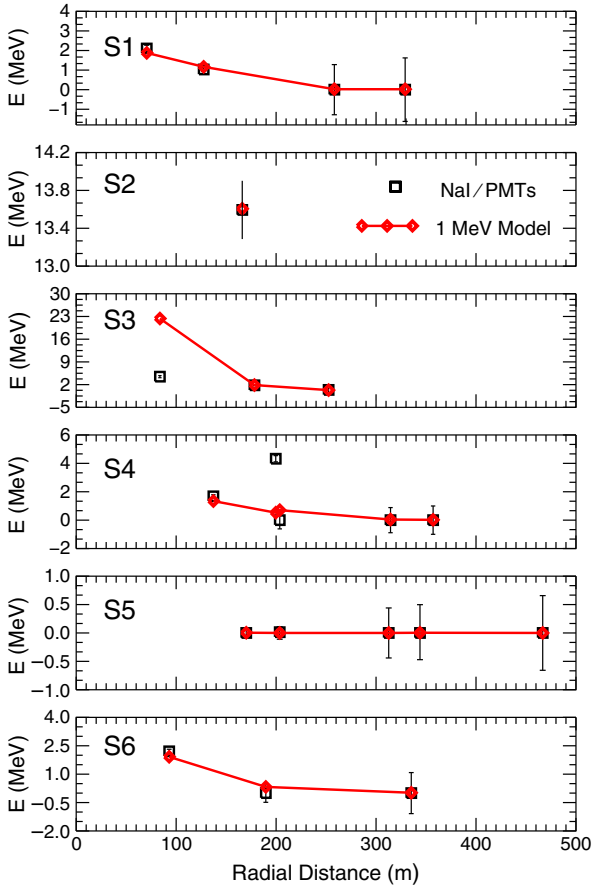

Figure 4. The radial energy distribution for each angular region for the X-ray burst labeled Q. S1 (short for Scale 1), S2, S3, S4, S5, and S6 can be visualized in Figure 2. Also, S1, S2, S3, S4, S5, and S6 contain 4, 1, 3, 5, 5, and 3 NaI/PMT detectors in each respective angular region. The black markers indicate the NaI/PMT detector energies radially outward from the launcher, while the red markers indicate what the model predicts. The fit of modeled and measured energies is the result shown.

but the question still remained whether individual X-ray bursts also produce isotropic electron and X-ray emission. To test this hypothesis, two complications needed to be addressed: the number of detected photons and the radial falloff of deposited energies. In order to complete the analysis, a minimum of 15 single photons (see Figure 2 time M for a single pulse that is probably a single photon) in each X-ray burst on the entire array had to be measured. This was determined by fitting the detector response function to the measured data and allows the photon energies to be extracted from the anode signal. Fitting the response function to the measured data can also help to separate pulses that overlap in time (see Figure 2, time H). If too few photons were measured, the statistical error becomes too high.

[22] In order to conduct this study and to produce sufficient statistics, three conditions within the data set needed to be met. Firstly, a majority (about 15 out of 24) of our TERA NaI/PMTs needed to be functioning. Secondly, X-ray bursts within each leader need to record a minimum of five X-ray pulses from the TERA NaI/PMT network. Thirdly, these X-ray bursts need to be well defined within a time step (a few microseconds). In other words, there cannot be a pileup of pulses lasting more than a few microseconds. An example of a large, extended set of piled up pulses can be seen in Figure 2 in the light blue colored pulses in time *T* and the red colored pulses in time *U*.

[23] Forty-four lightning leaders were analyzed in this study, but only five leaders contained X-ray bursts that satisfied the above conditions. Particularly, the data selected in this section involves only rocket-triggered leaders from 2007 and 2010, specifically flashes UF 07-07 on 31 July 2007, UF 10-06 on 17 June 2010, UF 10-20 on 15 July 2010, UF 10-23 on 31 July 2010, and UF 10-24 on 13 August 2010. These five leaders, composed of 21 leader X-ray bursts, displayed an adequate amount of data to form some preliminary conclusions about the anisotropy. Triggered leaders were chosen because the approximate electron source of the X-ray bursts is known to be around the launch location in the *xy* plane. The approximate altitude above the launcher can also be determined from the average leader speed, which was assumed to be on the order of 10^6 m s^{-1} for dart-stepped leaders and 10^7 m s^{-1} for dart leaders for four of the leaders investigated. Though these values are approximate leader speeds, which are input parameters for the model, they do not significantly affect the simulations results. The fifth leader's (UF 07-07 L1) average downward speed was determined through d*E*/d*t* TOA source locations [*Howard et al.*, 2010]. The X-ray bursts from these leaders were analyzed to determine their X-ray angular distribution.

[24] Each lightning leader was analyzed using the data from up to 21 NaI/PMT detectors. Only unshielded NaI/PMTs were used to produce all the following figures except one (Figure 8). Since NaI has a relatively long light-decay time constant of 0.23 μs, pulses tend to pile up (see Figure 2, the orange pulses in time O). For this reason, only the total deposited energy was attained with the NaI/PMTs in this analysis. This total deposited energy was calculated by measuring the amplitude of each X-ray pulse, which is then multiplied by a calibration factor to produce the corrected energy. By calibrating with five radioactive sources, it was found that the relationship between pulse height and energy remain linear up to 1.3 MeV. The linearity was not measured above 1.3 MeV, but it was assumed for this paper that it remained linear for higher energies (above 1.3 MeV) similar to the assumptions of *Dwyer et al.* [2012]. Using this assumption, the energies measured were calibrated with a Cs-137 (662 keV) radioactive source.

[25] To account for the radial falloff of deposited energies, due to the varying locations of the detectors for each individual leader, the time that X-rays were emitted from the leader channel was calculated, which is called the emission time. X-rays were identified as being from within the same burst if they contained the same emission time (within a few microseconds). It should be noted that occasionally, the modeled falloff of deposited energy does not fit the measured falloff of deposited energy well. This could be due to a more complicated emission pattern than supposed in the model or additional X-ray emission (possibly other leader branches that are not included in the model, although this scenario

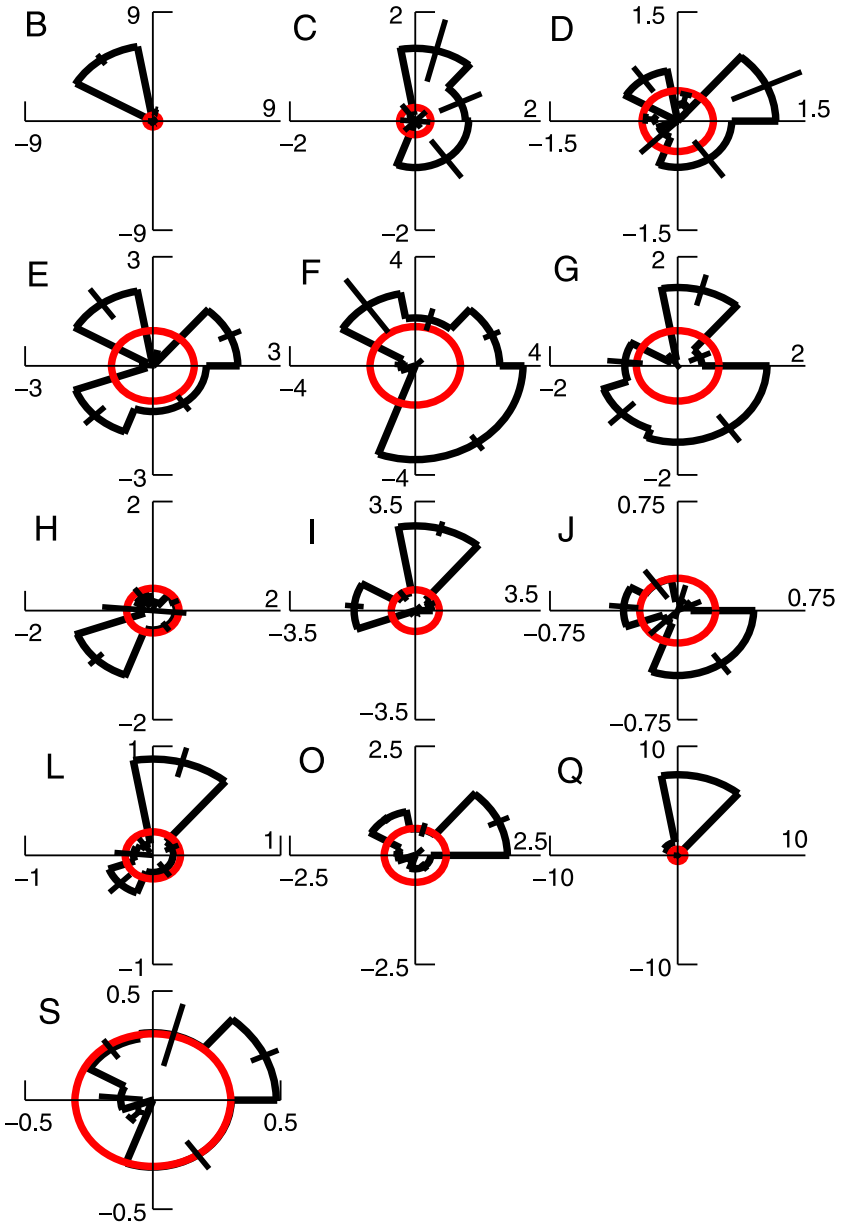

Figure 5. The angular distribution (in black) for each X-ray burst from the dart-stepped leader of UF 07-07. The red circles indicate a perfectly isotropic emission of X-rays.

is unlikely since additional branches are rare for triggered leaders). The emission time is calculated by subtracting the propagation time of the X-rays (assumed to be the speed of light) from the lightning channel to each TERA box. Fiber optic propagation delays are also accounted for since the X-ray source regions are moving at a significant fraction of the speed of light, and the duration of the lightning leader process only lasts a few microseconds. The time measured at the launcher at which the return-stroke current has risen to half of its peak value is defined as the observation time of $t = 0$.

[26] For each X-ray burst, the deposited energy on each detector was found. These detectors were divided into six azimuthal bins, with each bin containing at least one detector. The bins were 0–50°, 51–100°, 101–150°, 151–200°, 201–250°, and 251–359°, where 0° is in the east direction from the rocket launcher and increasing in angle when moving counter clockwise around the launcher (see Figures 3, 10, and 13). For each angular region, the deposited energy from the detectors was compared to the modeled radial energy distribution using the maximum likelihood technique (see Figure 4, which is explained in the next section) to determine the intensity of X-rays emitted in that angular region, thus accounting for the radial falloff of deposited energies. An e-folding energy of 1 MeV with an isotropic emission of electrons from the source region was used to produce the modeled energies.

[27] The likelihood function was constructed from the product of the Gaussian distributions for the n detectors with j possibilities:

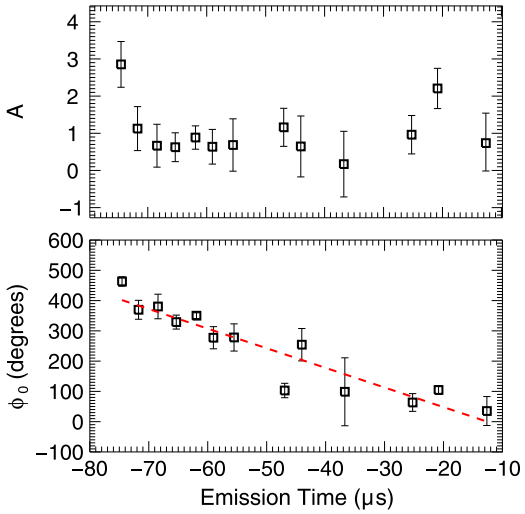

Figure 6. (top) The magnitude of anisotropy, A, and (bottom) the direction of anisotropy, ϕ_0, versus emission time for the X-ray bursts from UF 07-07 L1. The binned markers are X-ray bursts arranged as follows (left to right): B, C, D, E, F, G, H, I, J, L, O, Q, and S. (bottom) The red dashed line indicates the fit to the direction of anisotropy.

$$L_j = \prod_{i=1}^{n} \frac{1}{\sigma_i \sqrt{2\pi}} \exp\left\{-\frac{[E_{d,i} - a_j E_{m,i}]^2}{2\sigma_i^2}\right\}, \quad (1)$$

where $E_{d,i}$ and $E_{m,i}$ are the deposited energies detected on the NaI/PMTs and the energy expected in the model per X-ray burst for the ith detector, σ_i is the standard deviation from the model, and a_j is the fit parameter found by maximizing the likelihood function for the jth angular region [*Melissinos*, 1966]. Monte Carlo simulations were used to predict the number of photons detected because the exact number is not known in the measurements. Finding the number of photons allowed the Poisson errors to be calculated. To determine this Poisson error, the average modeled energy per photon for each of the TERA PMTs was used (which is then used in combination with the measured deposited energies to calculate the number of photons detected) rather than using the minimum measured photon count estimated by fitting the detector response function to the anode waveform (see *Saleh et al.* [2009] for more details). The minimum photon count was not used in this case because when fitting the detector response function to the measured data, the exact photon energies can only be extracted from the anode waveforms if the photons arrive at different times. If the photons arrive at exactly the same time, the anode signal will appear to be the characteristic shape of the NaI light pulse.

[28] The maximum of the likelihood function, $L_{\max}$ was found for each angular region, which determines the factor, a_j, that scales the modeled data to the measured energies. The error in a_j, σ_j, was also determined when maximizing the likelihood function. When $E_{m,i}$ is equal to $E_{d,i} + 1\sigma$, the likelihood function becomes approximately exp[–0.5]. Hence, a 1σ standard deviation of a_j is found when $L \approx L_{\max} \exp[-0.5]$. This method is computed for each angular region and X-ray burst that contains an adequate amount of photons and do not saturate any detectors (i.e., saturation will eliminate an entire X-ray burst). An example of a saturated pulse can be seen in Figure 2 at times R, T, and U. It should be noted that not including bursts with saturated tubes could introduce a bias.

[29] Two procedures were used to determine if the X-ray bursts were consistent with isotropic emission or if the bursts have some degree of anisotropy. The first procedure involved using the first-order harmonic function of the form

$$f(A, \phi_0) = B(1 + A\cos(\phi - \phi_0)), \quad (2)$$

where ϕ_0 is the most probable azimuthal direction of the anisotropy, A is the most likely magnitude of the anisotropy, and B is a constant. This method found the most probable magnitudes of the anisotropy and the directions of that anisotropy for each X-ray burst (see Tables 1–4). The magnitudes of anisotropy are also labeled as "significant anisotropy" or "not significant anisotropy" throughout this paper. When the error bars (in the magnitude of anisotropy) overlap zero anisotropy, this is defined to be significant anisotropy for this paper. To complete this procedure, the function, f, was fit to the measured scaling factors, a_j, using a χ^2 goodness-of-fit test. The parameters of A and ϕ_0 were set to vary until the χ^2 was minimized. The most probable values of A and ϕ_0 were determined where the χ^2 reached a minimum.

[30] For the second procedure, each scaling factor, a_i, and error, σ_i, was fit to a constant, C, to determine if the X-rays in the six angular regions were consistent with an isotropic emission using a χ^2 goodness-of-fit test. In other words,

$$\chi^2 = \sum_{i=1}^{n} \left\{-\frac{[a_i - C]^2}{\sigma_i^2}\right\}. \quad (3)$$

The χ^2 value combined with the degrees of freedom then determined the approximate probability, P, (from the χ^2 distribution) that the measured energies are consistent with an isotropic electron source of emission [*Melissinos*, 1966]. Once the values of χ^2 were found from the goodness-of-fit test, the confidence in the model, using a Monte Carlo procedure, was calculated using Pearson's χ_p^2 statistic following the approach of *Dwyer et al.* [2012]. The values of the χ^2

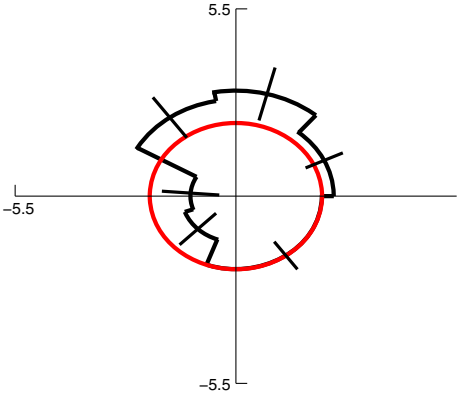

Figure 7. X-ray bursts B, C, D, E, F, G, H, I, J, L, O, Q, and S (between 80 and 0 μs) summed together to produce the total angular distribution from UF 07-07 L1.

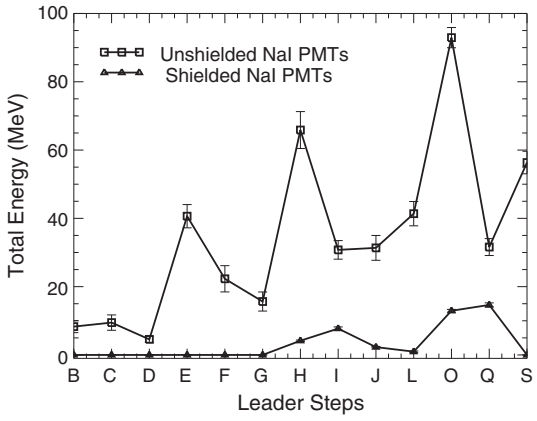

Figure 8. The difference in total energy between the unshielded and shielded NaI/PMTs for the X-ray bursts from UF 07-07.

were compared to the χ_p^2 distribution to calculate the probability, P_p, that $\chi^2 > \chi_p^2$ for the number of degrees of freedom. The fraction of the χ_p^2 values that were larger than the measured value gave an estimate of the significance in which the model may be rejected. Values less than this fraction of χ_p^2 can exclude the model with a significance given by the probability.

[31] To show that the statistical errors are not responsible for the results from procedure 1 or 2, we introduced a set of simulated data that has an isotropic distribution. Using the Monte Carlo simulation, a set of data, with K_0 = 1 MeV and electrons emitted isotropically, was created and analyzed using the 1 MeV isotropic model. This isotropic simulated data set resulted in no significant first-order anisotropy (A = 0.217 ± 0.409) and was determined to be consistent with an isotropic electron emission (χ_ν^2 = 0.443, P = 0.78). Additionally, a second simulated data set, using an anisotropic electron source, was also analyzed using the 1 MeV isotropic model. As expected, a significant first-order anisotropy (A = 1.11 ± 0.416) resulted, and the simulated anisotropic data set produced a probability (χ_ν^2 = 11.24, P = 0) that was not consistent with an isotropic source. Additionally, the choice of characteristic energy could, perhaps, be very important because of the irregular locations of the detectors. To determine if the magnitude of the characteristic energy has affected the azimuthal anisotropy results, two sets of simulated data were introduced to further test our procedures. First, we introduced a simulated isotropic model with K_0 = 300 keV and analyzed it using the 1 MeV model. As expected, the results were consistent with an isotropic source of emission (χ_ν^2 = 0.016, P = 0.9995), with no significant first-order anisotropy (A = 0.279 ± 0.41). The second test was to introduce another simulated model with K_0 = 300 keV instead of using a model with K_0 = 1 MeV to analyze burst Q. This resulted in significant first-order anisotropy (A = 0.977 ± 0.51) and inconsistency with an isotropic source (χ_ν^2 = 92.6, P = 0).

[32] A flowchart of the analysis can be found in Figure 1.

5. Results

[33] In the following section, results from five leaders, a total of 18 X-ray bursts, will be shown.

5.1. UF 07-07 Leader 1

[34] UF 07-07 L1, which was also analyzed in *Saleh et al.* [2009], was a triggered lightning dart-stepped leader that was measured on 31 July 2007. Its return-stroke peak current measured an amplitude of 45 kA. The deposited X-ray energy, averaging over all detectors, was shown to fit the empirical expression [exp(–r/120)]/r where r is the radial distance of the NaI/PMTs in meters [*Saleh et al.*, 2009]. The average background rate was found to be about 80 MeV/s on the unshielded detectors with the expected background energy to be at most 16 keV [*Saleh et al.*, 2009]. *Saleh et al.* [2009] showed that an average isotropic electron source (i.e., over the entire length of the lightning channel where X-ray production is occurring) fit better to the data than an average downward beamed electron source. The average downward speed was determined, by the use of dE/dt TOA source locations, to be 4.8×10^6 m s^{-1} [*Howard et al.*, 2010]. The e-folding energy was determined through Monte Carlo simulations to be about 1 MeV [*Saleh et al.*, 2009].

[35] The input parameters, found in *Saleh et al.* [2009], such as e-folding energy and leader speed, were used in the analysis that was explained above. Figure 2 shows the raw X-ray waveform converted into energy using a Cs-137 radioactive source. The corresponding dE/dt waveform (at station 7 located to the southwest of the launch tower) is also displayed. The timing has been adjusted to show emission time, so that the distinction between X-ray bursts can be displayed. The dashed lines segmenting the X-ray bursts indicate the approximate individual time lengths of each

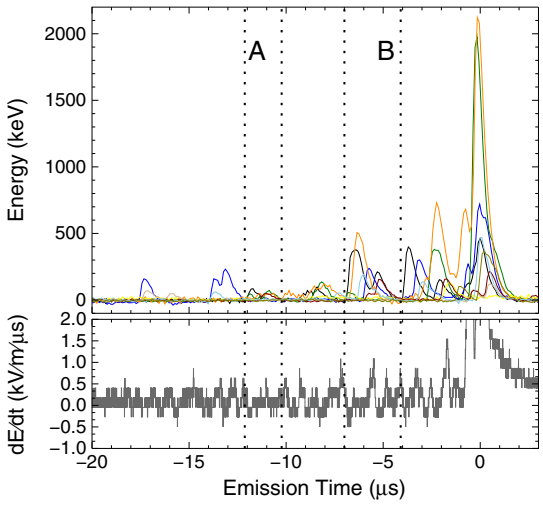

Figure 9. The waveform of X-ray from the dart leader UF 10-06 converted into energy using a Cs-137 radioactive source. The electric field derivative is displayed below the X-ray waveform. Each color of X-ray pulse displays a separate NaI/PMT detector. The timing has been adjusted to show emission time, so that the distinction between X-ray bursts can be seen. The dashed lines segmenting the X-ray bursts indicate the approximate individual time lengths of each X-ray burst, which were chosen to be about at the start and stop of the X-ray emission for each burst. The letters at the top of each X-ray burst segment indicate the time frame of each X-ray burst. Both times A and B were chosen to be analyzed.

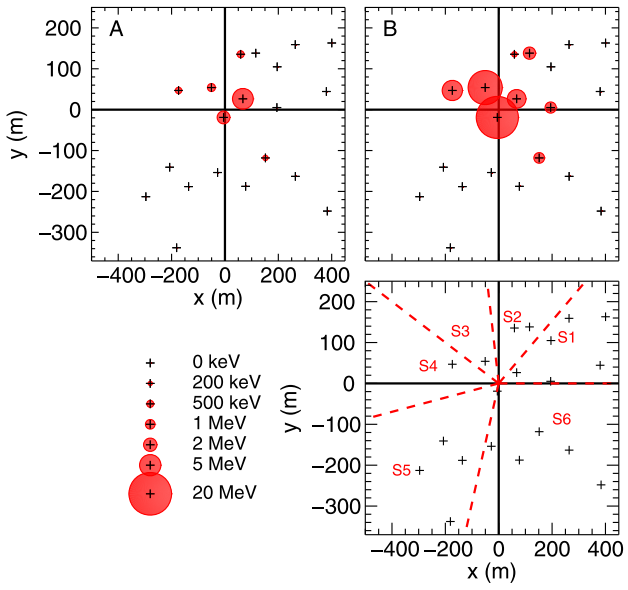

Figure 10. The spatial distribution of energies across the unshielded NaI/PMT detectors from the X-ray bursts of UF 10-06. The plus markers indicate the location of the TERA detectors across the ICLRT site. A north and east headings are labeled as *y* and *x*, respectively. The horizontal and vertical black lines at the origin show the position of the launcher. The red circles indicate the total energy deposited in each unshielded NaI/PMT with the area proportional to its energy. (bottom right) The dashed lines indicate which TERA PMTs are located in each azimuthal region (S1, S2, S3, S4, S5, and S6).

X-ray burst, which was chosen to be about at the start and stop of the X-ray emission for each burst. Not every X-ray burst can be seen on the measured d*E*/d*t* waveform, but several sharp d*E*/d*t* pulses are displayed in coincidence with X-ray emission. The letters at the top of each X-ray burst segment indicate the time frame of each X-ray burst and will be referred to later in this paper. Times B–H, I, J, L, O, Q, and S were chosen to be analyzed. The remainder of these times show saturation in the X-ray pulses or show too few X-ray pulses to be analyzed.

[36] Figure 3 shows the spatial distribution of energies across the unshielded NaI/PMT detectors. The plus markers indicate the location of the TERA detectors across the ICLRT site. A north and east headings are labeled as *y* and *x*, respectively. The horizontal and vertical black lines at the origin show the origin of the launcher. The red circles indicate the total energy deposited in each unshielded NaI/PMT with the area proportional to its energy. Not all NaI/PMT detectors display deposited energies during each X-ray burst. During some leader bursts, the X-ray emission is stronger in certain directions (e.g., X-ray burst Q has higher energies on the NaI/PMTs north of the launcher). Also, as time progresses, the energies in the NaI/PMTs during each X-ray burst increases.

[37] Figure 4 shows the radial energy distribution for each angular region for the leader burst labeled Q. The angular regions, S1 (short for Scale 1), S2, S3, S4, S5, and S6, can be visualized in Figure 3 (bottom right). Also, S1, S2, S3, S4, S5, and S6 contain 4, 1, 3, 5, 5, and 3 NaI/PMT detectors in each respective angular region. The black markers indicate the PMT energies radially outward from the launcher, while the red markers indicate what the model predicts. The fit of the modeled and measured energies is the result shown in Figure 4. In other words, the modeled energies are scaled to fit the measured energies. Each angular region contains its own scale and error, which was calculated using the maximum likelihood technique as described in section 4. In S2 and S5, markers with zero energy are displayed. This results from PMTs that measured no X-rays below 30 keV (the lower PMT sensitivity limit). A similar approach was completed for the remainder of the angular regions.

[38] For each X-ray burst, the scale distribution (determined from the fit of the modeled and the measured energies) is shown in Figure 5. For each of the angular regions, the scale and the error (shown as a radial error bar in each region) is shown in black. The red circles indicate a perfectly isotropic emission of X-rays. The arrows, which in some cases are very close to zero making them difficult to

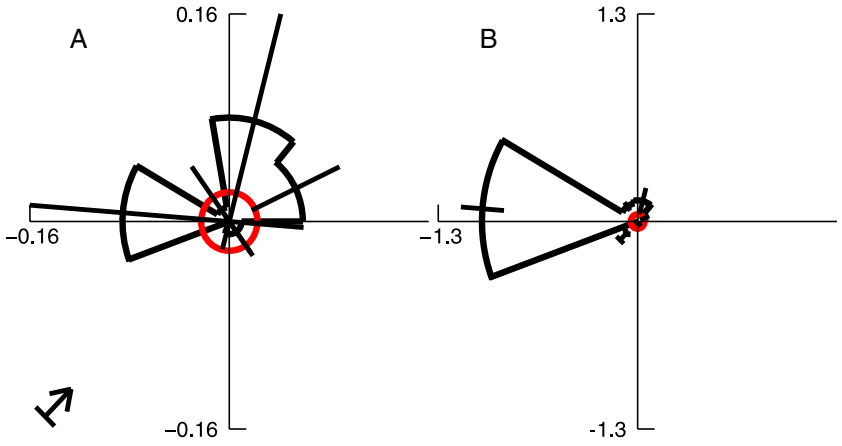

Figure 11. The angular distribution (in black) for each X-ray burst from the dart leader of UF 10-06. The red circles indicate a perfectly isotropic emission of X-rays. The arrows in both plots indicate the upper limit of the scaling factor in its angular region if the detection of photons had occurred.

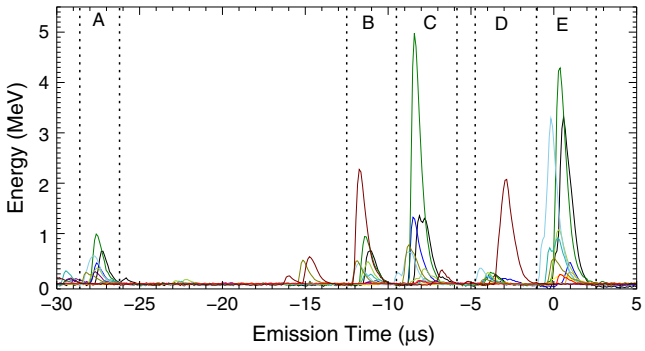

Figure 12. The last 30 μs of the X-ray waveform from the unshielded NaI/PMTs from the dart-stepped leader UF 10-23 converted into energy using a Cs-137 radioactive source. The electric field derivative was not available for this dart leader. Each color of X-ray pulse displays a separate NaI/PMT detector. The timing has been adjusted to show emission time, so that the distinction between X-ray bursts can be seen. The dashed lines segmenting the X-ray bursts indicate the approximate individual time lengths of each X-ray burst, which were chosen to be about at the start and stop of the X-ray emission for each burst. The letters at the top of each X-ray burst segment indicates the time frame of each burst. Times A–D were chosen to be analyzed. X-ray burst E shows saturation and was excluded.

be seen on the scale in Figure 5, display upper limits where no X-ray detection occurred. Almost all X-ray bursts show some degree of anisotropy when looking at Figure 5. Table 1 shows the χ^2_ν, χ^2 probability distribution (P), the Pearson probability (P_p), the magnitude of anisotropy (A), and the azimuthal direction of anisotropy (ϕ_0) results for each X-ray burst. Based on Figure 6, which uses procedure 1, and Table 1, all bursts except two have significant first-order anisotropy. The probabilities from procedure 2 also agree that all bursts investigated from UF 07-07 are inconsistent with an isotropic emission.

[39] Figure 6 (bottom) shows the azimuthal direction of the anisotropy for UF 07-07 L1. It is interesting to note that the direction of anisotropy appears to decrease in angle from –80 μs to –10 μs. A linear function (seen as a dashed line in Figure 6, bottom) was fit to the directions of anisotropy to determine the Pearson correlation coefficient, which indicates the strength of the linear relationship between the linear function and the direction of anisotropy. The strength of the linear relationship increases as the coefficient approaches 1. The correlation coefficient, in this case, was 0.941, indicating a good correlation.

[40] The anisotropy is shown in an alternate form in Figure 7. By summing up the normalized scaling factors from the X-ray bursts B, C, D, E, F, G, H, I, J, L, O, Q, and S, the total angular distribution can be seen for UF 07-07 L1. This Figure has significant anisotropy even when the emission is averaged over 80 μs.

[41] Figure 8 shows the difference in total energy between the unshielded and shielded NaI/PMTs for the X-ray bursts investigated in UF 07-07 L1. Since the shielded detectors are surrounded by 0.3175 cm thick lead, they become transparent to X-ray energies greater than about 200 keV. A general increase in energy occurs as the X-ray bursts approach the ground with the unshielded detectors. This also can be seen in Figure 3. Only during later times (leader bursts closer to the start of the return stroke) do individual energies start to increase.

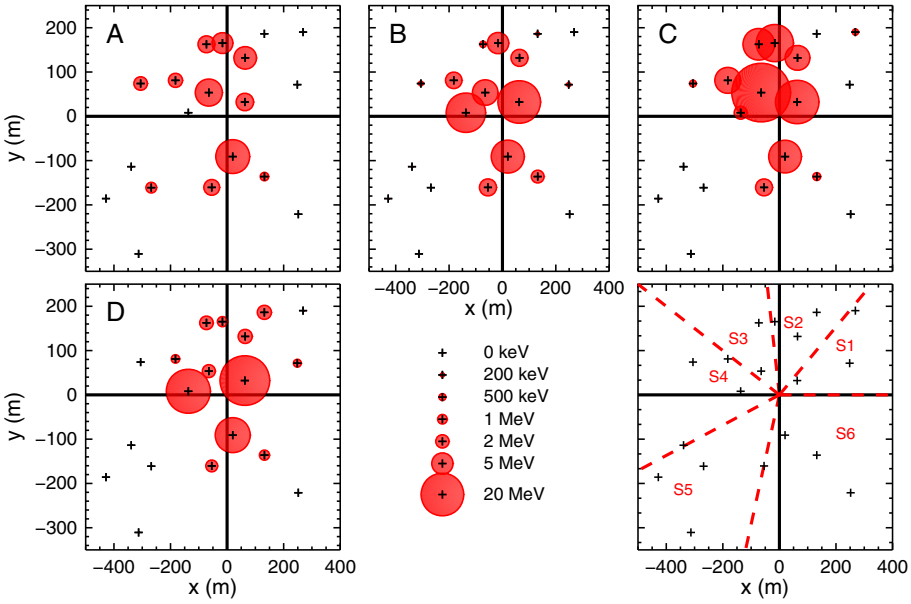

Figure 13. The spatial distribution of energies across the unshielded NaI/PMT detectors from the X-ray bursts of UF 10-23. The plus markers indicate the location of the TERA detectors across the ICLRT site. A north and east headings are labeled as y and x, respectively. The horizontal and vertical black lines at the origin show the position of the launcher. The red circles indicate the total energy deposited in each unshielded NaI/PMT with the area proportional to its energy. (bottom right) The dashed lines indicate which TERA PMTs are located in each azimuthal region (S1, S2, S3, S4, S5, and S6).

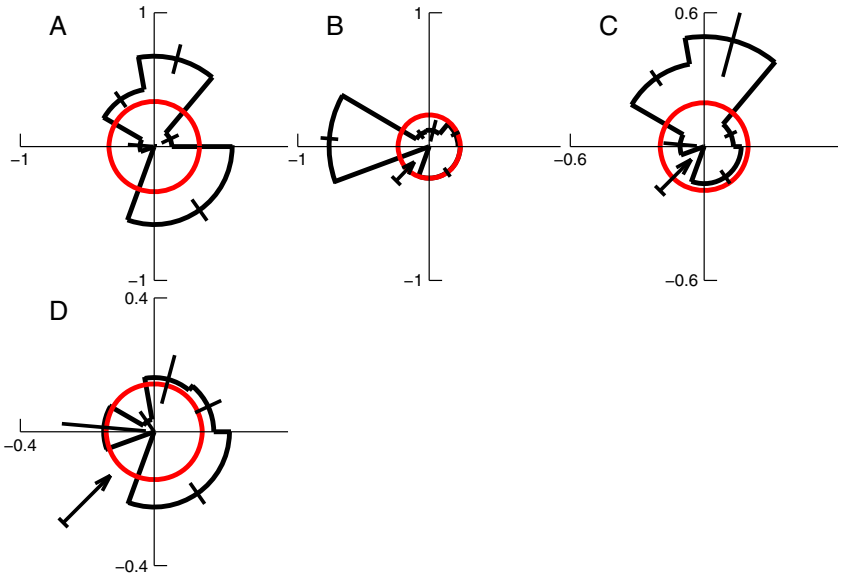

Figure 14. The angular distribution (in black) for each X-ray burst from the dart-stepped leader of UF 10-23. The red circles indicate a perfectly isotropic emission of X-rays. The arrows display upper limits where no X-ray detection occurred.

5.2. UF 10-06 Leader 1

[42] UF 10-06 leader 1, a dart leader with a small "chaotic" component close to the initiation of the return stroke, triggered on 17 June 2010, was the first leader of an eight-leader/return-stroke sequence. Its return-stroke peak current measured an amplitude of about 15 kA. For this leader, two X-ray bursts were investigated and the average downward leader speed was approximated to be on the order of 10^7 m s^{-1}. Figure 9 shows the emission times of the X-ray and dE/dt waveforms of these X-ray bursts. Figure 10 displays the spatial distribution of energies over the ICLRT site similar to Figure 3. Once again, the black lines at the origin indicate the location of the launcher and the plus markers are the locations of the unshielded detectors. Larger energies are displayed on PMTs closer to the launcher. Not all PMTs show detection of X-rays. Figure 11 shows the angular distribution of scales similar to Figure 5. The errors are much larger on X-ray burst A due to the lower number of X-ray pulses. The arrows in both plots indicate the upper limit of the scaling factor in its angular region if the detection of photons had occurred. According to both procedures, X-ray burst A is consistent with the isotropic emission. For burst B, procedure 1 does not find a significant first-order anisotropy. However, procedure 2 shows that the emission is not consistent with the isotropic model due to higher-order anisotropies. Table 2 shows the χ^2_ν, P values, A, and ϕ_0 for X-ray bursts A and B.

5.3. UF 10-23 Leader 16

[43] UF 10-23 L16, a dart-stepped leader triggered on 31 July 2010, was the sixteenth leader of a 16-leader/return-stroke sequence. Its return-stroke peak current measured an amplitude of about 20.2 kA. Figure 12 shows the last 30 μs of the X-ray waveform from the unshielded NaI/PMTs. The electric field derivative was not measured for this leader. A–D indicate the X-ray bursts used in the analysis. X-ray burst E shows saturation and was excluded. Figures 13 and 14 are analyzed using the same method as Figures 3 and 5. The largest deposited energies are displayed in X-ray burst C with energies over 20 MeV (see Figure 13). According to Table 3, all X-ray bursts show χ^2_ν and P values in combination with P_p that are inconsistent with an isotropic electron source model. Using procedure 1, all bursts do not have a significant first-order anisotropy, but higher-order anisotropies may be present. For example, X-ray burst A has a bipolar emission of X-rays (Figure 14). In other words, burst A does not have a significant first-order anisotropy but

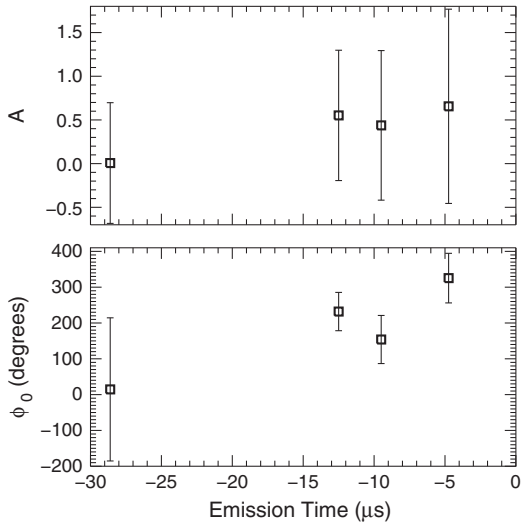

Figure 15. (top) The magnitude of anisotropy, A, and (bottom) the direction of anisotropy, ϕ_0, versus emission time for the X-ray bursts from UF 10-23 L16. The binned markers are X-ray bursts arranged as follows (left to right): A, B, C, and D.

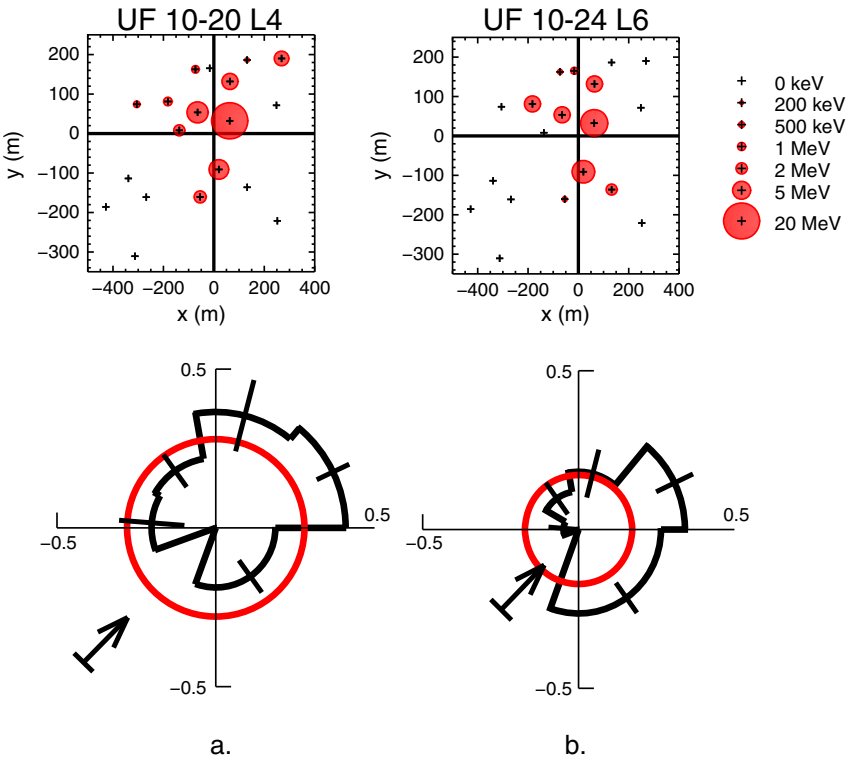

Figure 16. (top) The spatial distribution of energies across the unshielded NaI/PMT detectors from the X-ray bursts of (a) UF 10-20 L4 and (b) UF 10-24 L6. The plus markers indicate the location of the TERA detectors across the ICLRT site. A north and east headings are labeled as *y* and *x*, respectively. The horizontal and vertical black lines at the origin show the position of the launcher. The red circles indicate the total energy deposited in each unshielded NaI/PMT with the area proportional to its energy. The measured angular distribution (in black on the bottom) for each X-ray burst from the dart-stepped leaders of UF 10-20 (Figure 16a) and UF 10-24 (Figure 16b). The red circles indicate a perfectly isotropic emission of X-rays. The arrows show the upper limits where no X-ray detection occurred.

does display a second-order anisotropy. Figure 15 shows the approximate A and ϕ_0 for UF 10-23 L16.

5.4. UF 10-20 Leader 4 and UF 10-24 Leader 6

[44] This section will briefly discuss two dart-stepped leader X-ray bursts analyzed in this study. UF 10-20 L4 and UF 10-24 L6 contained return-stroke peak currents of 11.7 kA and 14.8 kA, respectively. The time frame investigated for UF 10-20 L4 was from –0.654 μs prior to the start of the return stroke to 1.917 μs after the start of the return stroke. The time frame investigated for UF 10-24 L6 was from –19.6 to –16.46 μs prior to the start of the return stroke. Plots similar to Figures 3 and 5 are shown in Figure 16. The associated χ^2_ν, probabilities, A, and ϕ_0 are shown in Table 4. Both of these X-ray bursts are statistically inconsistent with an isotropic X-ray emission but do not have a first-order anisotropy. It should be noted that higher-order anisotropies may be present.

6. Discussion

[45] Procedure 1 found the first-order anisotropy, and procedure 2 tested whether or not the angular distribution was consistent with an isotropic distribution. Because higher-order anisotropies could be present in the data, a distribution that is not isotropic does not necessarily have a significant first-order anisotropy. This was the case for bursts A-D from UF 10-23 L16, both of the bursts from UF 10-20 L4 and UF 10-24 L6, and burst B from UF 10-06 L1. Of those cases, second-order anisotropy can be seen in two bursts. In contrast, pronounced first-order anisotropy occurs in 11 of the 13 X-ray bursts from the dart-stepped leader of UF 07-07.

[46] All together, we find that 11 out of 21 X-ray bursts have a statistically significant first-order anisotropy, and hence those 11 are inconsistent with an isotropic emission. The remaining 10 bursts do not have significant first-order anisotropy. However, of those 10 bursts, 1 burst shows consistency with an isotropic distribution, while 9 are inconsistent with isotropic emission. These nine bursts do not have first-order anisotropy but do have significant higher-order anisotropy. The presence of discrete X-ray bursts suggests that stepping is involved since it is well-established that X-ray bursts are associated with the stepping process [*Dwyer et al.*, 2004a, 2005]. This refutes the hypothesis, implied by *Saleh et al.* [2009], that electron and X-ray emission from leaders bursts are all isotropic.

[47] Interestingly, for UF 07-07 L1, the orientation of this anisotropy seems to move in a spiraling motion in the clockwise direction around the vertical channel as seen in Figure 6, suggesting a "lighthouse" effect in the X-ray emission. If this is the case, the rotational rate of the X-ray emission would be about one rotation completed in 55 μs.

[48] It should be noted that the leader encounters the remnants of the vaporized wire around the emission time of –60 to –50 μs. Since the average speed of this dart-stepped leader is $4.8 \times 10^6\,\mathrm{m\,s^{-1}}$ [see *Howard et al.*, 2010], the approximate tip of the rocket-triggered vaporized wire (usually located between 200 and 300 m in altitude) could be located around the –60 to –50 μs emission time, and yet the orientation of the anisotropy continues in a spiraling motion after encountering the remnants of the wire.

[49] Furthermore, *Saleh et al.* [2009] inferred an average isotropic electron source over the leader channel from UF 07-07 L1 near the ground. This average deposited energy was determined over approximatively 1 ms of X-ray data. As shown in Figure 7, which contained X-ray data averaged over about 80 μs, the emission has a significant first-order anisotropy ($A = 0.347 \pm 0.277$, $\phi_0 = 46.56° \pm 13.38°$), in contrast to the isotropic emission inferred in *Saleh et al.* [2009] by averaging 1 ms of data. Since *Saleh et al.* [2009] did not consider anisotropies in the azimuthal direction, these new measurements of anisotropy do not necessarily contradict *Saleh et al.* [2009]. Indeed, our analysis supports the finding that the X-ray emissions from lightning are inconsistent with a vertically downward beam.

[50] Since most X-ray bursts (which are associated with the stepping process) have significant anisotropies, this may imply that the electron population on these electric field lines is not uniform. For instance, if the emission is due to runaway electron production at streamer heads, then either the number or intensity of streamers may not be uniform in the streamer zone. Another possibility is that the leader channel was not vertical (even though the electric field may be symmetrical around the channel), causing an anisotropy in the direction that the leader channel was tilted. This could be either from a tilting of the channel or random fluctuations in the leader directions around the average direction of the channel. Further work is needed to distinguish these various possibilities.

[51] Finally, a general increase in energy in the unshielded and shielded detectors occurs as the X-ray bursts approach the start of the return stroke as seen in Figure 6. This is in agreement with *Dwyer et al.* [2004a, 2005] and *Schaal et al.* [2012], who also noticed an increased intensity as the leader propagated toward the ground. This could be due to an increase in the electric field strength as the leader approaches the ground due to its image charge and to less Compton scattering by air because the X-rays propagate through less medium when near the ground than at higher altitudes.

[52] **Acknowledgments.** We would like to thank those at Florida Tech and the University of Florida who assisted in the maintenance and operation of TERA. Special thanks are extended to Ismael Diaz for all of the helpful discussions. This work was supported in part by NASA grant NNX09AJ07H and DARPA grants HR0011-08-1-0088 and HR0011-1-10-1-0061.

References

Beasley, W. H., M. A. Uman, D. M. Jordan, and C. Ganesh (1983), Simultaneous pulses in light and electric field from stepped leaders near ground level, *J. Geophys. Res.*, *88*, 8617–8619.

Cooray, V., and S. Lundquist (1985), Characteristics of the radiation fields from lightning in Sri Lanka in the tropics, *J. Geophys. Res.*, *90*, 6099–6109.

Dwyer, J. R., et al. (2003), Energetic radiation produced during rocket-triggered lightning, *Science*, *299*, 694–697.

Dwyer, J. R., et al. (2004a), Measurements of X-ray emission from rocket-triggered lightning, *Geophys. Res. Lett.*, *31*, L05118, doi:10.1029/2003GL018770.

Dwyer, J. R. (2004), Implications of X-ray emission from lightning, *Geophys. Res. Lett.*, *31*, L12102, doi:10.1029/2004GL019795.

Dwyer, J. R., et al. (2005), X-ray bursts associated with leader steps in cloud-to-ground lightning, *Geophys. Res. Lett.*, *32*, L01803, doi:10.1029/2004GL021782.

Dwyer, J. R., and D. M. Smith (2005), A comparison between Monte Carlo simulations of runaway breakdown and terrestrial gamma-ray flash observations, *Geophys. Res. Lett.*, *32*, L22804, doi:10.1029/2005GL023848.

Dwyer, J. R. (2007), Relativistic breakdown in planetary atmospheres, *Phys. Plasmas*, *14*, 042901, doi:10.1063/1.2709652.

Dwyer, J. R. (2008), *Energetic Radiation and Lightning: Principles, Instruments, and Applications, Review of Modern Lightning Research,* pp. 331–346, Springer, Netherlands, doi:10.1007/978-1-4020-9079-0.

Dwyer, J. R., D. M. Smith, M. A. Uman, Z. Saleh, B. Grefenstette, B. Hazelton, and H. K. Rassoul (2010), Estimation of the fluence of hight-energy electron bursts produced by thunderclouds and the resulting radiation doses received in aircraft, *J. Geophys. Res.*, *115*, D09206, doi:10.1029/2009JD012039.

Dwyer, J. R., D. M. Smith, and S. A. Cummer (2012), High-energy atmospheric physics: Terrestrial gamma-ray flashes and related phenomena, *Space Sci. Rev.*, *173*, 133–196, doi:10.1007/s11214-012-9894-0.

Dwyer, J. R., M. M. Schaal, E. Cramer, S. Arabshahi, N. Liu, H. K. Rassoul, J. D. Hill, D. M. Jordan, and M. A. Uman (2012), Observation of a terrestrial gamma-ray flash at ground level in association with a cloud-to-ground lightning return stroke, *J. Geophys. Res.*, *117*, A10303, doi:10.1029/2012JA017810.

Gorin, B. N., V. I. Levitov, and A. V. Shkilev (1976), Some principles of leader discharge of air gaps with a strong non-uniform field, *Gas Discharge, IEE Conf. Publ.*, *143*, 274–8.

Gurevich, A. V. (1961), On the theory of runaway electrons, *Sov. Phys. JETP*, *12*(5), 904–912.

Gurevich, A. V., G. M. Milikh, and R. A. Roussel-Dupré (1992), Runaway electron mechanism of air breakdown and preconditioning during a thunderstorm, *Phys. Lett. A*, *165*, 463–468.

Gurevich, A. V., and K. P. Zybin (2001), Runaway breakdown and electric discharges in thunderstorms, *Physics-Uspekhi*, *44*, 1119.

Howard, J., M. A. Uman, J. R. Dwyer, D. Hill, C. Biagi, Z. Saleh, J. Jerauld, and H. K. Rassoul (2008), Co-location of lightning leader X-ray and electric field change sources, *Geophys. Res. Lett.*, *35*, L13817, doi:10.1029/2008GL034134.

Howard, J., M. A. Uman, C. Biagi, D. Hill, J. Jerauld, V. A. Rakov, J. R. Dwyer, Z. H. Saleh, and H. K. Rassoul (2010), RF and X-ray source locations during the lightning attachment process, *J. Geophys. Res.*, *115*, D06204, doi:10.1029/2009JD012055.

Hill, J. D., M. A. Uman, D. M. Jordan, J. R. Dwyer, and H. K. Rassoul (2012), "Chaotic" dart leaders in triggered lightning: Electric fields, X-rays, and source locations, *J. Geophys. Res.*, *117*, D03118, doi:10.1029/2011JD16737.

Hill, J. D. (2012), The Mechanisms of Lightning Leader Propagation and Ground Attachment, Ph.D. Dissertation, University of Florida.

Kitagawa, A. (1957a), On the electric field change due to the leader processes and some of their discharge mechanism, *Pap. Meteor. Geophys. Tokyo*, *7*, 400–414.

Kochkin, P. O., C. V. Nguyen, A. P. J. van Deursen, and U. Ebert (2012), Experimental study of hard X-rays emitted from meter-scale positive discharges in air, *J. Phys. D: Appl. Phys.*, *45*, 425202, doi:10.1088/0022-3727/45/42/425202.

Krider, E. P., and G. J. Radda (1975), Radiation field waveforms produced by lightning stepped leaders, *J. Geophys. Res.*, *80*, 2653–2657.

Krider, E. P., C. D. Weidman, and R. C. Noggle (1977), The electric field produced by lightning leader steps, *J. Geophys. Res.*, *82*, 951–960.

Lehtinen, N. G., T. F. Bell, and U. S. Inan (1999), Monte Carlo simulation of runaway MeV electron breakdown with application to red sprites and terrestrial gamma ray flashes, *J. Geophys. Res.*, *104*, 24,699–24,712, doi:10.1029/1999JA900335.

Melissinos, A. C. (1966), *Experiments in Modern Physics*, Academic Press College Division, San Diego, CA.

Moore, C. B., K. B. Eack, G. D. Aulich, and W. Rison (2001), Energetic radiation associated with lightning stepped-leaders, *Geophys. Res. Lett.*, *28*, 2141–2144.

Moss, G. D., V. P. Pasko, N. Liu, and G. Veronis (2006), Monte Carlo model for analysis of thermal runaway electrons in streamer tips in transient luminous events and streamer zones of lightning leaders, *J. Geophys. Res.*, *111*, A02307, doi:10.1029/2005JA011350.

Rakov, V. A., and M. A. Uman (2003), *Lightning Physics and Effects*, Cambridge Univ. Press, Cambridge, United Kingdom.

Saleh, Z., J. Dwyer, J. Howard, M. Uman, M. Bakhtiari, D. Concha, M. Stapleton, D. Hill, C. Biagi, and H. Rassoul (2009), Properties of the X-ray emission from rocket-triggered lightning as measured by the Thunderstorm Energetic Radiation Array (TERA), *J. Geophys. Res.*, *114*, D17210, doi:10.1029/2008JD011618.

Schaal, M. M., J. R. Dwyer, Z. H. Saleh, H. K. Rassoul, J. D. Hill, D. M. Jordan, and M. A. Uman (2012), Spatial and energy distributions of X-ray emissions from leaders in natural and rocket triggered lightning, *J. Geophys. Res.*, *117*, D15201, doi:10.1029/2012JD017897.

Suszcynsky, D. M., R. Roussel-Dupré, and G. Shaw (1996), Ground-based search for X-rays generated by thunderstorms and lightning, *J. Geophys. Res.*, *101*(23), 23,505–23,516.